Int Ophthalmol (2019) 39:2223–2235
https://doi.org/10.1007/s10792-018-01061-w

ORIGINAL PAPER

The involvement of the mGluR5-mediated JNK signaling pathway in rats with diabetic retinopathy

Yan-Ni Zhu · Guo-Jin Zuo · Qi Wang · Xiao-Ming Chen · Jin-Kui Cheng · Shu Zhang

Received: 7 May 2018 / Accepted: 21 December 2018 / Published online: 3 January 2019

Abstract

Objective To understand the involvement of the mGluR5-mediated JNK signaling pathway in rats with diabetic retinopathy (DR).

Methods This study established rat models of diabetes mellitus (DM), which were divided into Normal, DM, DM + CHPG (mGluR5 agonist CHPG), and DM + MTEP (mGluR5 antagonist MTEP) groups. The blood glucose and weight of rats were recorded. EB staining was used for observation of blood–retinal barrier (BRB) damage. Neural retina function was measured by pattern electroretinogram (ERG). PAS and NG2 immunohistochemistry were conducted to evaluate the retinal vascular morphology. The TUNEL assay and active caspase-3 immunohistochemistry were performed to detect retinal cell apoptosis. Additionally, the expression levels of superoxide dismutase (SOD) and methylenedioxyamphetamine (MDA) were measured. Moreover, expression levels of mGluR5 and JNK pathway-related proteins were detected by western blot.

Results When compared with control rats, rats in the DM group showed decreased amplitude and latency of the peak times in the ERG test; further, DM group rats presented increases in blood glucose, BRB permeability, a retinal capillary area density, retinal cell apoptosis with an increased number of active caspase-3-positive cells, MDA level, mGluR5 levels, and the ratio of p-JNK/JNK, and they showed reductions in body weight and SOD activity, as well as in the number of pericytes and in the pericyte coverage (all $P < 0.05$). However, rats in DM + CHPG group had stronger negative effects than those in DM group (all $P < 0.05$). Rats from DM + MTEP group showed an opposite trend compared with the DM rats (all $P < 0.05$).

Conclusion The level of mGluR5 in DR rats was upregulated, whereas inhibition of mGluR5 alleviated retinal pathological damage and decreased cell apoptosis to improve DR via suppression of the JNK signaling pathway, which provided a scientific theoretical basis for the clinical treatment of DR.

Keywords mGluR5 · JNK signaling pathway · Diabetes mellitus · Diabetic retinopathy · Apoptosis

Introduction

As one of the most serious but common microvascular complications of diabetes, diabetic retinopathy (DR) is considered globally as a major cause of blindness [1], with approximately 93 million patients with DR and 28 million patients with vision-threatening diabetic retinopathy (VTDR) worldwide [2]. The pathogenesis of DR is very complex, involving various biochemical

Y.-N. Zhu (✉) · G.-J. Zuo · Q. Wang · X.-M. Chen · J.-K. Cheng · S. Zhang
Department of Ophthalmology, Jingzhou First People's Hospital, Jingzhou, Hubei, China
e-mail: yanni_zhu35412@sina.com

pathways including the activation of the polyol pathway, abnormality in the diestroglycerin and protein kinase C signaling pathways, accumulation of late glycation end products, oxidative stress reactions, and inflammatory responses [3, 4]. Although many therapeutic drugs exist which could target the above pathways, DR treatment is still not satisfactory [3]. Therefore, it is of substantial importance to further study the underlying mechanism of DR.

Glutamate is recognized as an important and major excitatory neurotransmitter in the retina, and its uptake is crucial for normal transmission at glutamatergic synapses [5]. However, abnormal glutamate metabolism occurs in diseases, such as retinitis pigmentosa and glaucoma, in which the excitatory toxic effect caused by increased glutamate levels results in activated glutamate receptors [6]. As a vitally important neurotransmitter receptor in the nervous system, glutamate receptors include ionic glutamate receptors (iGluRs) and metabolic glutamate (mGluRs) [7]. The mGluRs can be divided into the following three types: type I (which includes mGluR1 and mGluR5), type II (which includes mGluR2, mGluR3, and mGluR7), and type III (which includes mGluR4, mGluR6, and mGluR8) [8]. Recently, evidence pointed out that mGluR5 is activated in a glaucoma model, in which it could regulate the introvert potassium current to further affect the expression of Kir4.1 [6, 9]. Additionally, mGluR5 in brain neurons can significantly activate the JNK signaling pathway in the study of Yang et al. [10]. In terms of JNK, it is a mitogen-activated protein kinase (MAPK) superfamily member [11], which can be widely implicated in various biological processes, such as apoptosis, proliferation, metabolism, transportation, and DNA damage repair, through activation of a wide range of extracellular stimulation factors, such as growth factors and cytokines [12, 13]. More importantly, the JNK signaling pathway has been confirmed to be upregulated in DR and to exert a vital function in DR development [10]. However, only limited data are available regarding the role of mGluR5 in DR. Therefore, this study attempted to understand the involvement of mGluR5 in regulating the JNK signaling pathway in rats with DR, thereby providing novel ideas for the prevention and treatment of DR.

Materials and methods

Ethics statement

The animal experimental design in this study was approved by the Experimental Animal Ethics Committee of the First People's Hospital of Jingzhou; all experimental animal behaviors strictly followed the laboratory animal management and operation guide issued by National Institutes of Health [14].

Preparation of diabetes mellitus (DM) rat models and grouping

A total of 60 8-week-old Sprague–Dawley (SD) rats (weight: 200–250 g) were purchased from Shanghai Sippr-BK Laboratory Animal Co. Ltd. (Shanghai, China). All the animals in the laboratory had adaptive feeding for 1 week at room temperature of 21 ± 2 °C with free food and water in accordance with the light rhythm of 12-h daylight and 12-h darkness. After 12-h fasting, 45 rats were randomly selected to accept an intraperitoneal injection of 60 mg/kg streptozotocin (STZ) (Sigma-Aldrich Corporate, Louis, Missouri, USA) [15] to induce the DM rat model. After 72 h, the blood glucose was detected by a Johnson rapid glucometer using the oxidase test paper method from the tail tip, and rats with blood glucose of > 16.7 mmol/l were identified as DM rats [16]. The remaining 15 rats were injected with normal saline of equal volume and served as the Normal group. The successfully constructed DM rat models were divided into three groups with 15 rats in each group as follows: the DM + CHPG group [in which 300 μmol mGluR5 agonist CHPG was injected into the vitreous cavity (Sigma-Aldrich Corporate, Louis, Missouri, USA)]; the DM + MTEP group [in which an injection of 150 nmol mGluR5 antagonist MTEP was injected into the vitreous cavity (Sequoia Research Products, Pangbourne, UK)]; and the DM group (in which phosphate buffer solution (PBS) of the same volume was injected into the vitreous cavity). The rats in each group received daily treatments for 16 weeks. The monthly measurement of body weight and fasting blood glucose was performed for 16 weeks.

Evaluation of blood–retinal barrier (BRB) damage

After 16 weeks of treatment, an intraperitoneal injection of pentobarbital sodium salt (18 mg/kg) and an intramuscular injection of xylazine hydrochloride (0.19 ml/kg) were given to rats, as described in previous research [17], which was followed by an intravenous injection of Evans blue (EB, 45 mg/kg) within 1 min. Two hours later, 1% paraformaldehyde diluted by preheated citrate buffer (37 °C) was perfused via the left ventricle for 2 min. Then, the eyeball was removed immediately, and rats were killed by cutting their necks. Next, the retina was saved in the refrigerator at 4 °C overnight to measure the dry weight. After the retina was incubated with 150 µl formamide at 70 °C for 8 h, the extracted solution was kept in a 1.5-ml ultrafiltration centrifuge tube and centrifuged at 6000 r/min at 4 °C for 90 min. The absorbance value of the supernatant was measured using a microplate reader, and the differences between absorbance values of samples at 620 nm and 740 nm were determined. Based on a standard curve of EB, we calculated the concentrations of EB in the dry retinas and plasma. The calculation of BRB breakdown was done by the following formula: BRB breakdown = EB µg/retina dry weight (g)/time − averaged EB concentration (µg/ml/h) [18].

Electroretinogram (ERG)

Briefly, rats were dark-adapted overnight. ERG responses were recorded from both eyes together using platinum wire corneal electrodes, a forehead reference electrode, and a ground electrode in the tail. Pupils were fully dilated using 1% tropicamide solution (Alcon). Methylcellulose (Celluvisc, Allergan, Irvine, CA) drops were applied as well to maintain a good electrical connection, and the body temperature was maintained at 37 °C by a water-based heating pad. ERG waveforms were recorded with a bandwidth of 0.3–500 Hz, and samples were taken at 2 kHz by a digital acquisition system and were analyzed by a custom-built program (MATLAB). Statistics were done on the mean ± SD amplitudes of the a- and b-wave of each group.

HE staining

The rat eyeball was fixed with 4% paraformaldehyde, dehydrated by gradient alcohol, embedded in paraffin, and cut into a series of 5-µm-thick slices. First, a slice was dewaxed by xylene, dehydrated with gradient ethanol, and stained with hematoxylin for 6 min, followed by running water wash for 10 min. After differentiation by 1% hydrochloric acid alcohol for 15 s, the slice was rinsed by a trickle of water and counterstained with eosin for 3 min. Upon dehydration with gradient ethanol and transparency by xylene, the slice was sealed in neutral gum. The morphological changes in the retina were observed under an optical microscope.

Periodic acid–Schiff (PAS) staining

The retinal vascular network was removed to make retinal vasculature stretched preparation. With washing by tap water, stretched preparation was treated with high-iodide solution. After being stained with Schiff solution, the stretched preparation was stained with Harris hematoxylin, washed with running water, and differentiated with HE staining differentiation solution for 30 s. Finally, with dehydration and transparency by xylene, the stretched preparation was fixed in neutral gum. Under a microscope, the retinal vessels were observed.

Detection of apoptosis by the terminal deoxynucleotidyl transferase (TdT)-mediated dUTP nick end labeling (TUNEL) assay

Paraffin sections were dewaxed and dehydrated routinely, and tissues were treated with proteinase K at room temperature for 10 min. After washing with TBS (Tris-buffered saline), each specimen was mixed with labeling buffer and placed in a wet box at 37 °C. The section was sealed for 30 min, followed by the addition of biotin–digoxin–FITC antibody for a 30-min incubation at 37 °C prior to sealing with mounting medium containing DAPI (4′, 6-diamidino-2-phenylindole) (Sigma-Aldrich Corporate, Louis, Missouri, USA). The computer image system software Image Tool version 1.0 was applied to count the number of apoptotic cells.

Immunohistochemistry

Sections were treated with 0.3% H_2O_2 to block endogenous peroxidase. After washing with PBS, sections were blocked with PBS containing 0.1% normal horse serum and 0.4% Triton-X 100 for 1 h at room temperature. They were then incubated overnight at 4 °C with a rabbit polyclonal antibody against active caspase-3 (1:10,000; R&D Systems, Minneapolis, MN) and anti-NG2 (1:500, Millipore). The sections were then incubated with secondary antibodies for 30 min and visualized with a diaminobenzidine substrate kit (DAKO).

For NG2 staining, retinas were dissected from the eye and incubated in blocking solution (0.5% Triton-X-100, 1% BSA in PBS) for 3 h at room temperature. Retinas were stained with the biotinylated isolectin B4 (1:50; Vector) or anti-NG2 (1:500, Millipore) primary antibodies at 4 °C overnight in PBLEC (1% Triton-X 100, 1 mM $MgCl_2$, 1 mM $MnCl_2$, and 1 mM $CaCl_2$ in PBS [pH 6.8]). After washing with PBLEC, retinas were incubated with Alexa Fluor-conjugated secondary antibodies (1:500, Invitrogen) in PBLEC. Stained retinas were flat mounted in 90% glycerol, and confocal stacked images were acquired using a Nikon A1R microscope. Quantification of pericyte coverage was performed using ImageJ on four 10 × confocal stacked images per retina.

Detection of the oxidative stress index

After treatment, 3.2% w/v sodium citrate was used to collect fresh arteriopuncture blood samples, and then samples were put into a vacutainer to run a centrifugation at 3500 rpm/min for 10 min. On the basis of instructions given by the producer, colorimetric assay kits (Cayman Chemicals, Ann Arbor, MI, USA) were applied to measure superoxide dismutase (SOD) activity and methylenedioxyamphetamine (MDA) levels in retinas, and the blood samples were calculated via plotted standard curves at 450 nm.

Western blot

The retinal tissue protein in each group was extracted separately, and the concentration of extracted protein was determined according to the procedures of a BCA (bicinchoninic acid) kit (Beyotime Biotechnology Co., Shanghai, China). After the addition of loading buffer, the extracted protein was boiled at 95 °C for 10 min. A total of 30 μg samples were loaded in each well to separate protein via 10% polyacrylamide gel (Wuhan Boster Biological Technology Ltd., Wuhan, Hubei, China) electrophoresis. After the protein was transferred onto the PVDF membrane, the membrane was sealed by 5% bovine serum albumin (BSA) at room temperature for 1 h. Then, the membrane was incubated with one of the following primary antibodies at 4 °C overnight: mGluR5 (1:1000), p-JNK (1:1000), JNK (1:1000), or β-actin (1:2000). All primary antibodies were purchased from Cell Signaling Technology, MA, USA. After TBST washing three times (5 min per wash), the membrane was incubated with a secondary antibody at room temperature for 1 h. After washing three times (5 min per wash), the membrane was developed by chemiluminescence reagent, including β-actin as an internal reference. The gray value of the target band was analyzed using ImageJ software.

Statistical analysis

All collected data were processed by SPSS 21.0 software (SPSS, Inc., Chicago, IL, USA). The measurement data were represented as the mean ± standard deviation ($\bar{x} \pm s$). The comparisons between two groups and among multiple groups were made by *t* test and one-way ANOVA separately. The P value of < 0.05 was considered as statistically significant.

Results

Body weight, blood glucose, and ERG outcomes in rats

Figure 1a shows the changes in body weight and blood glucose in rats from each group at different time points. The normal rats had enhanced body weight with the increase in feeding time, but the body weight increased slowly in rats from the DM, DM + CHPG, and DM + MTEP groups compared with the normal rats at the same corresponding time point (all $P < 0.05$). Meanwhile, the body weight was greatly decreased in rats of the DM + CHPG group but evidently increased in those of the DM + MTEP group when compared with DM rats at the corresponding time point (all $P < 0.05$). In addition, the

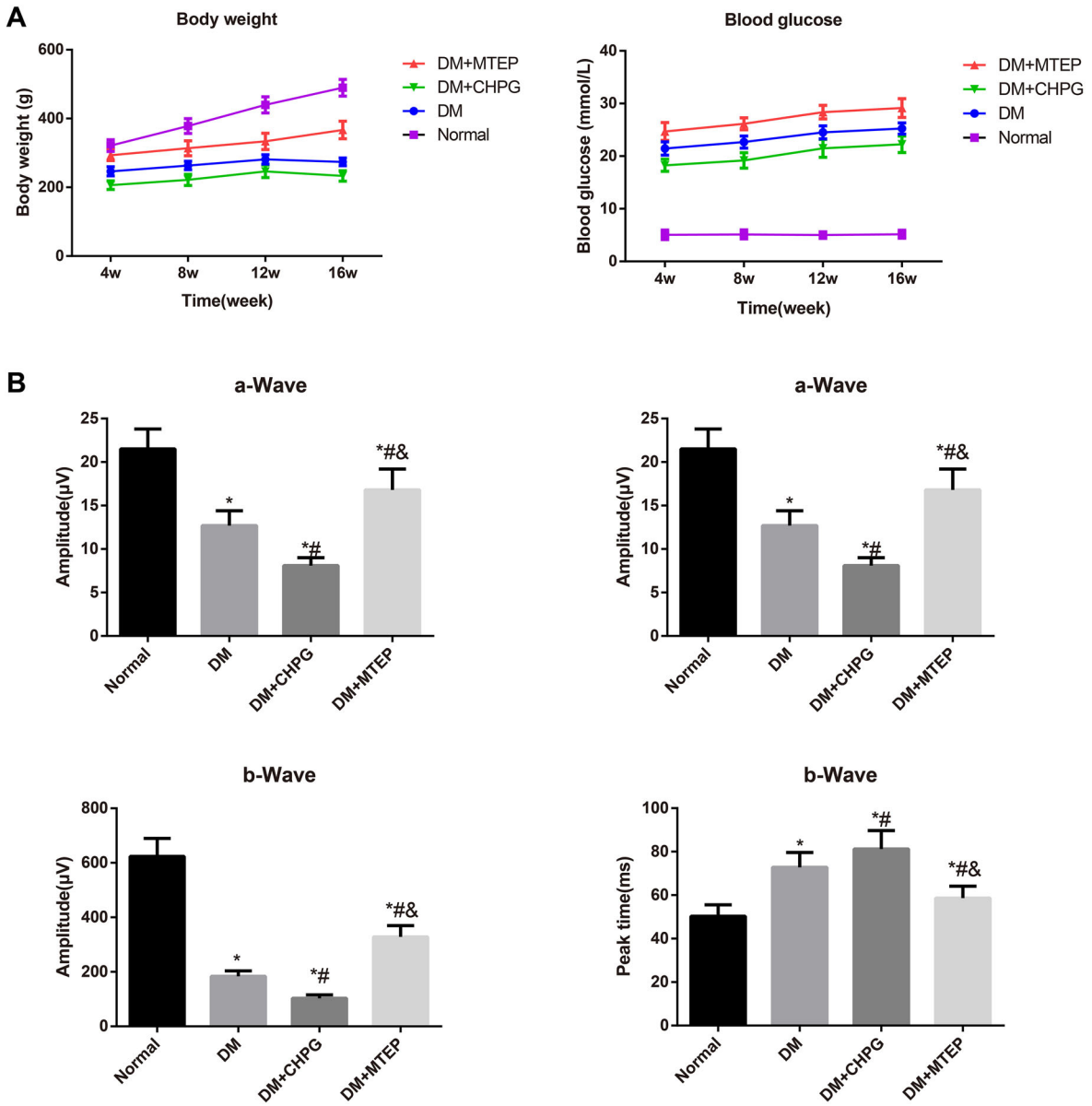

Fig. 1 The changes in body weight, blood glucose (**a**) and ERG amplitude and peak time (**b**) in rats from each group at different time points. *Notes* $^{*}P < 0.05$, compared with the Normal group; $^{\#}P < 0.05$, compared with the DM group; $^{\&}P < 0.05$, compared with the DM + CHPG group

blood glucose level was normal in normal rats and had no changes during the experiment. However, the blood glucose level in rats from the three other groups was significantly increased when compared with normal rats at the corresponding time points (all $P < 0.05$). Specifically, the blood glucose level showed a sharp increase in rats from the DM + CHPG group and a dramatic decrease in rats from the DM + MTEP group when compared with those from the DM group at the corresponding time points (all $P < 0.05$). In the ERG test (Fig. 1b), DM rats showed significantly declined amplitude and latency of the peak times compared with normal rats (all $P < 0.05$). Changes in the DM + CHPG group were larger compared with the DM group (all $P < 0.05$). Additionally, MTEP treatment increased amplitude and shortened peak times compared with DM group (all $P < 0.05$).

Observation of HE staining and BRB breakdown in rats under a light microscope

The rats' retinal pathological changes were observed by using HE staining. The retinal tissue of normal rats was in a complete structure and had a smooth internal limiting membrane with clear layers. Additionally, ganglion cells were round or oval, stained lightly, and arranged in a layer. All the retinal layers were closely arranged in order and clear. In rats from the DM group, there was visible swelling and thickening in the internal retinal membrane, part of which was broken, and there was an ambiguous boundary. Additionally, some retinal cells were vacuolated with nuclear condensation and dissolution, and the rats from the DM + CHPG group presented more substantial results. In Fig. 2a, the retinopathy in rats from the DM + MTEP group was greatly relieved in contrast to DM rats, and the retinal layer was relatively clear with a mildly swollen inner boundary film and a small number of vacuolar cells. As shown in Fig. 2b, when compared with rats in the Normal group, the BRB permeability in DM rats increased significantly ($P < 0.05$). In contrast to the DM group, the BRB permeability significantly increased in rats from the DM + CHPG group, but it decreased critically in rats from the DM + MTEP group (both $P < 0.05$).

Observation of PAS staining in rats

The morphological distribution of the retinal vascular network in rats was observed by PAS staining. The normal rats had a complete retinal vascular network, and the retinal vascular endothelial cells were lightly stained with bigger oval nuclei; the pericytes were strongly stained and had small nuclei in the shape of a circle or triangle. In the DM group, the rats' capillaries were closed, and they had hamartomatous proliferation of vascular endothelial cells, which formed a crescent, fusiform, and polygon; this resulted in capillary hemangioma, and the more serious effects were observed in rats from the DM + CHPG group. However, the retinal vascular network was distributed more symmetrically, along with vessels in orderly arrangement and vessels in a more consistent diameter, in rats from the DM + MTEP group, which lacked obvious swelling, proliferation, or deformation of the microvessels (Fig. 3a). As shown in Fig. 3d, e, the area density of retinal capillaries was significantly increased, but the number of pericytes was decreased in the DM group in contrast to the Normal group (all $P < 0.05$). Compared with the DM group, the DM + CHPG group showed an obvious increase in the area density of retinal capillaries and a decrease in the number of pericytes, but the DM + MTEP group presented the opposite trend, namely decreased area density of retinal capillaries and an increased number of pericytes (all $P < 0.05$). To visualize pericyte coverage, we performed confocal imaging of whole-mount retinas stained for NG2 to mark pericytes and isolectin B4 to label the endothelium. The capillary endothelium of the normal rats was continuously lined by NG2-positive pericytes (Fig. 3b). In contrast, gaps in pericyte coverage were observed in the retinal

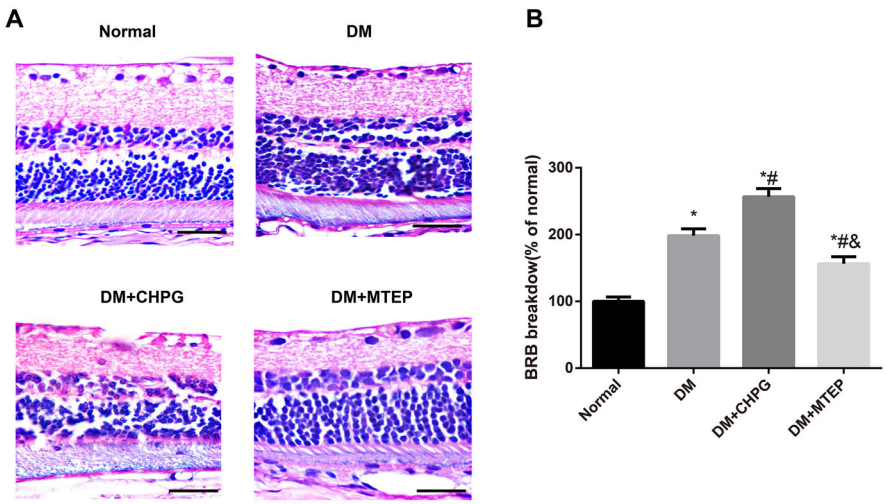

Fig. 2 The observation of rats' retinal pathological changes by using HE staining (**a**) and BRB breakdown (**b**) under a light microscope (× 200, scale bar: 50 μm). *Notes* $^{*}P < 0.05$, compared with the Normal group; $P < 0.05$; $^{\#}P < 0.05$, compared with the DM group; $^{\&}P < 0.05$, compared with the DM + CHPG group

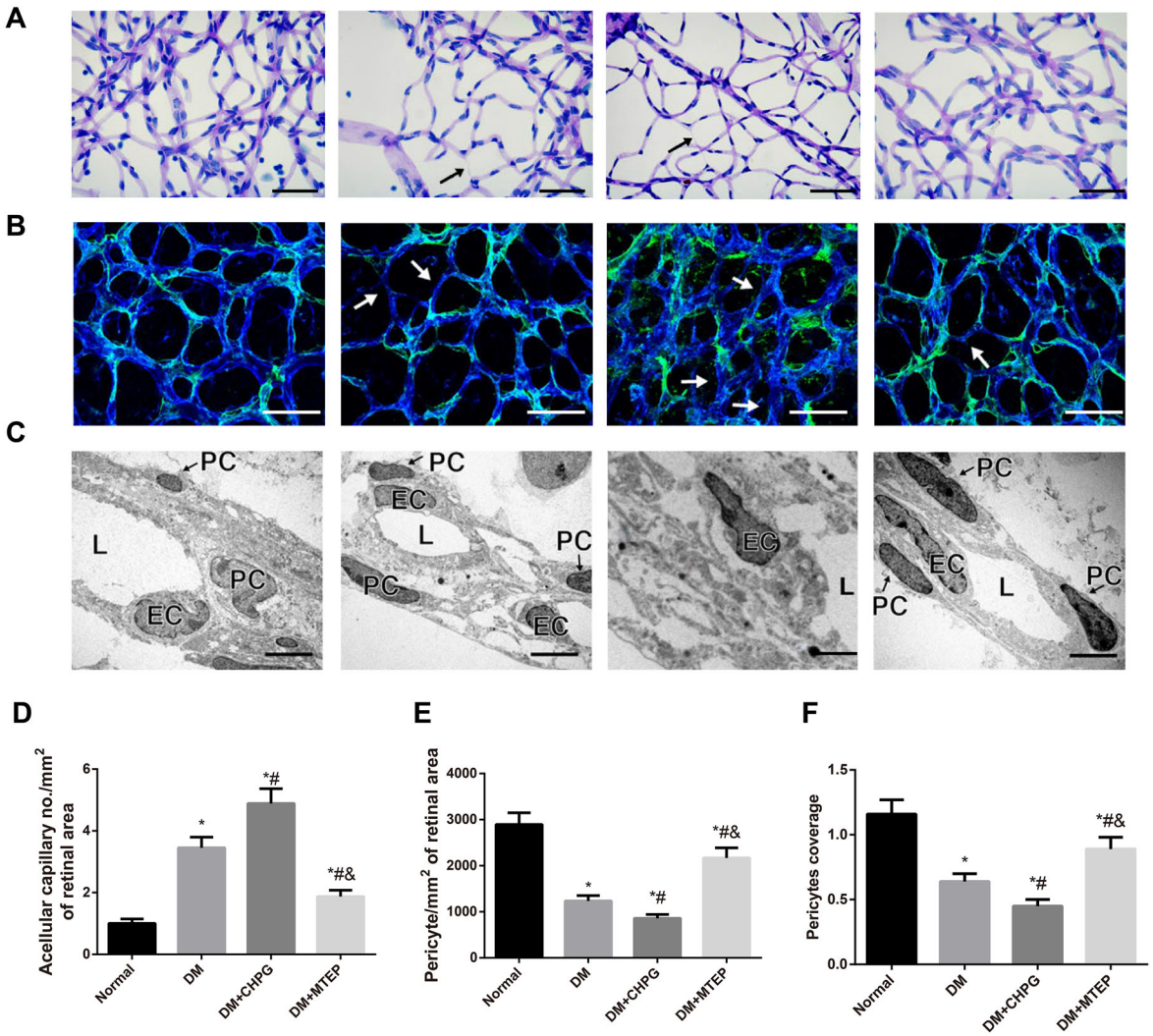

Fig. 3 The observation of the morphological distribution of retinal vascular network in rats. *Notes* **a** Typical photomicrographs detected by using PAS staining under a light microscope (× 400, scale bar: 50 μm). Black arrows indicate an acellular capillary; **b** immunohistochemistry for isolectin B4 (blue) to mark endothelial cells and NG2 (green) to mark pericytes (scale bar: 25 μm). White arrows mark endothelium devoid of pericyte coverage; **c** electron micrographs of retinal capillaries show vessel lumen (L), endothelial cell nuclei (EC), and pericytes nuclei (PC). Pericytes were marked by black arrows. Scale bar: 1 μm. **d–f** Quantification of acellular capillary segment/mm^2 (**d**), pericytes/mm^2 of capillary area in the retinal vessels (**e**), and vascular pericyte coverage (**f**); $^*P < 0.05$, compared with the Normal group; $P < 0.05$; $^{\#}P < 0.05$, compared with the DM group; $^{\&}P < 0.05$, compared with the DM + CHPG group

capillaries of DM rats, as defined by sections of endothelium devoid of an overlaying NG2-positive signal. Quantification of NG2 staining relative to vascular density showed reduced pericytes coverage in retinas of DM rats compared with normal rats (Fig. 3f). In contrast to the DM group, the pericyte coverage was significantly decreased in rats from the DM + CHPG group but was increased in rats from the DM + MTEP group (both $P < 0.05$). To gain a deeper understanding of the interaction between pericytes and the endothelium, we employed electron microscopy to visualize pericyte/endothelial cell associations in the vessel wall of retinal capillaries. Electron micrographs of rats showed a normal capillary vessel wall, with pericytes tightly lining the blood vessels (Fig. 3c). DM rats displayed altered vessel structures with pericytes located at a greater distance from the vessel lumen, indicative of pericyte

dissociation; the changes were more notable in the DM + CHPG group, but fewer changes were observed in the DM + MTEP group.

Retinal apoptosis of rats in each group

The retinal apoptosis of rats in each group was observed by the TUNEL assay. As presented in Fig. 4a, c, the retinal inner nuclear layer (containing the Muller and bipolar cell bodies) and the ganglion cell layer (containing retinal ganglion cells) had very few apoptotic cells in the Normal group but had a large number of apoptotic cells in the DM and DM + CHPG groups. Compared with the Normal group, a sharp increase in apoptotic cells was observed in the DM and DM + CHPG groups (both $P < 0.05$). In contrast to the DM group, the DM + CHPG group had a greater increase in apoptotic cells ($P < 0.05$). The number of apoptotic cells that were found in the DM + MTEP group was significantly less than the number observed in the DM group ($P < 0.05$). Immunohistochemical analysis showed many active caspase-3-positive cells in the inner retina in DM rats compared with normal rats ($P < 0.05$, Fig. 4b, d). The number of active caspase-3-positive cells was apparently increased in the DM + CHPG group, but the number was decreased in the DM + MTEP group compared with the DM group (both $P < 0.05$).

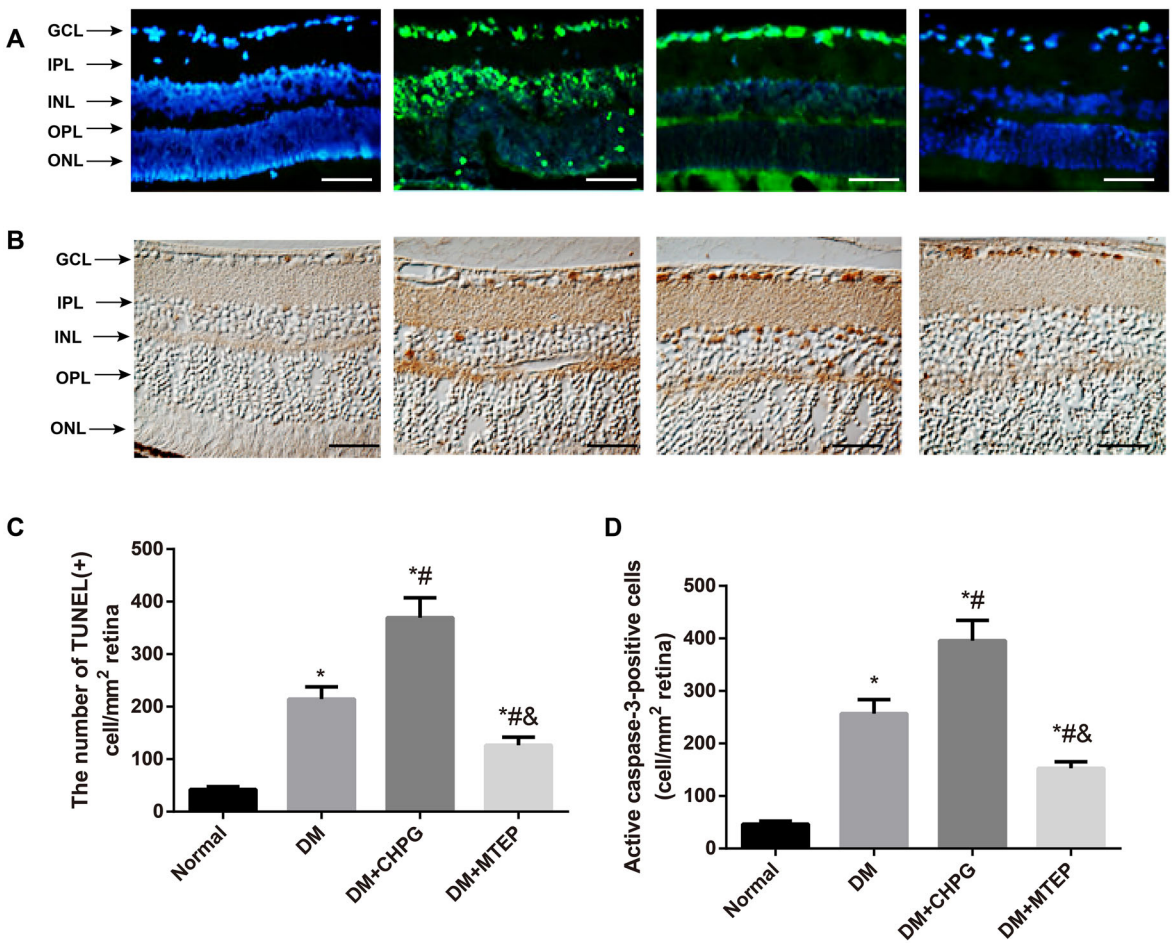

Fig. 4 Comparison of retinal apoptosis and expression of active caspase-3 of rats in each group. *Notes* **a** TUNEL staining, the apoptotic cells were labeled with green fluorescence and the nuclei of cells were stained with blue fluorescence (DAPI) (× 200, scale bar: 50 μm); **b** immunoreactivity for active caspase-3 was observed in the inner retina (× 200, scale bar: 50 μm); *GCL* ganglion cell layer, *INL* inner nuclear layer, *IPL* inner plexiform layer, *OPL* outer plexiform layer, *ONL* outer nuclear layer. **c**, **d** Quantification of the TUNEL (+) cells (**c**) and active caspase-3-positive cells (**d**). $^{*}P < 0.05$, compared with the Normal group; $P < 0.05$; $^{\#}P < 0.05$, compared with the DM group; $^{\&}P < 0.05$, compared with the DM + CHPG group

Comparison of the oxidative stress-related index in each group

As shown in Fig. 5, significantly decreased SOD activity and greatly raised MDA levels were found in the serum and retinal tissues of rats from the DM group compared with normal rats (both $P < 0.05$). Furthermore, in contrast to the DM group, rats in the DM + CHPG group showed an evident reduction in SOD activity and a great increase in MDA level in serum and retinal tissue, while those in the DM + MTEP group presented an opposite result of obviously increased SOD and a sharply decreased MDA level (all $P < 0.05$).

Expression levels of mGluR5 and JNK pathway-related proteins in rat retinal tissues

The expressions of mGluR5 and JNK pathway-related proteins in the retinal tissues of rats from each group were detected by western blot. As shown in Fig. 6, both the mGluR5 protein expression level and p-JNK/JNK ratio were significantly upregulated in DM rats compared with normal rats (both $P < 0.05$). Moreover, both mGluR5 protein expression level and p-JNK/JNK ratio were evidently increased in rats from the DM + CHPG group (both $P < 0.05$) but were sharply reduced in those from the DM + MTEP group, compared with DM rats (both $P < 0.05$).

Discussion

To our knowledge, STZ-induced diabetic rat is accepted as one of the commonly used models of diabetes, as well as an economical and reliable animal model to study DR [19]. In the current research, the DM rat model was successfully constructed via an intraperitoneal injection of STZ and treated with mGluR5 agonist (CHPG) or antagonist (MTEP) for 16 weeks; the retinal vascular dilation and lumen occlusion were observed by using HE staining and PAS staining, respectively, showing that the diabetic rats developed severe retinopathy, which is consistent with the results of previous studies [18, 20]. Retinal capillaries have been identified to contain three parts, including capillary basement membrane, endothelial

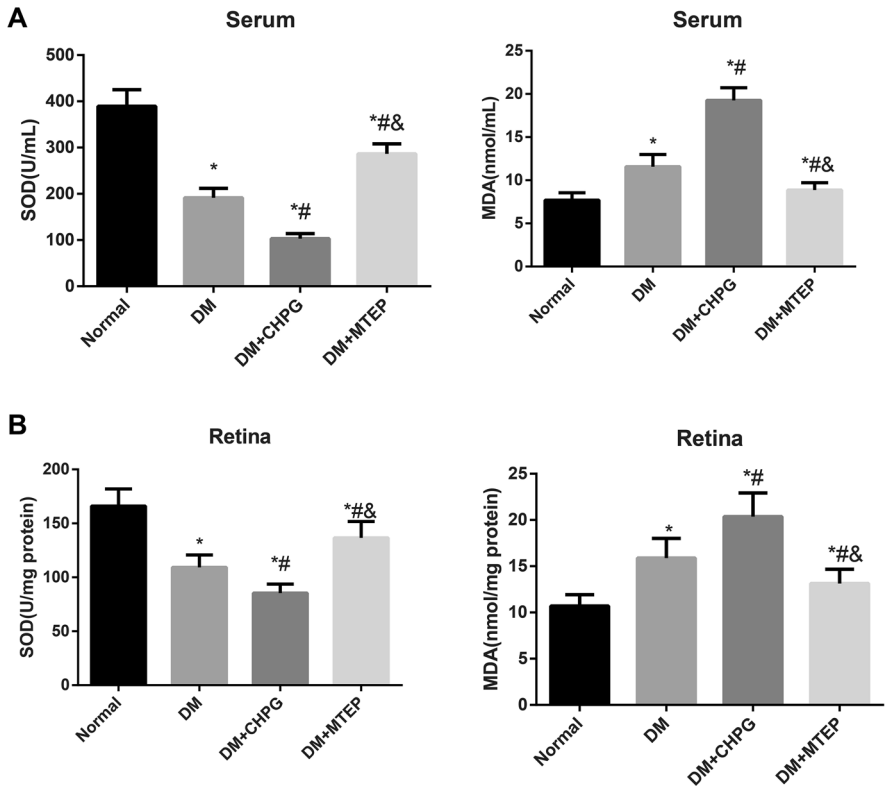

Fig. 5 Comparison of the SOD activity and MDA level in the serum (**a**) and retinal tissues (**b**) of rats in each group. *Notes* $^{*}P < 0.05$, compared with the Normal group; $P < 0.05$; $^{\#}P < 0.05$, compared with the DM group; $^{\&}P < 0.05$, compared with the DM + CHPG group

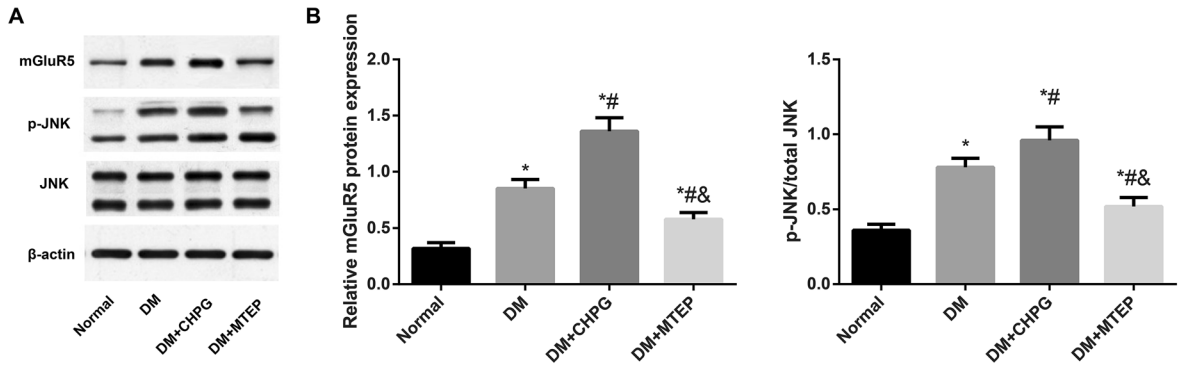

Fig. 6 The expression levels of mGluR5 and the JNK pathway-related proteins in the retinal tissues of rats from each group, detected by western blot. *Notes* **a** The expression levels of mGluR5 and the JNK pathway-related proteins in the retinal tissues of rats were detected by western blot; **b** comparison of the expression of mGluR5 and the JNK pathway-related proteins in each group; $^{*}P < 0.05$, compared with the Normal group; $P < 0.05$; $^{\#}P < 0.05$, compared with the DM group; $^{\&}P < 0.05$, compared with the DM + CHPG group

cells, and pericytes [21]. Among them, pericytes can regulate the local blood flow and vessel permeability owing to their systolic functions; thus, the selective loss of pericytes is indicative of the earliest pathological change in DR [22, 23]. Moreover, the BRB damage caused by the long duration of hyperglycemia strengthens the aggregation of blood platelets, increases blood viscosity, slows down blood flow velocity, and blocks the retinal capillary, which results in retinal ischemia and hypoxia, as well as in the decline in the retinal blood vessel elasticity and the increase in the capillary peripheral resistance, further promoting the development of DR [24, 25]. Accordingly, our study showed a great elevation of the area density of retinal capillaries with decreased pericytes, as detected by PAS staining; further, an evident strengthening of BRB permeability, as detected by EB staining in rats, was observed in the DM group [26]. Of note, the retinal pathological damage was further aggravated in DM rats treated with CHPG, while those DM rats treated with MTEP presented improved vasodilatation, decreased capillary area density, less loss of pericytes, and alleviated BRB, suggesting that the activation of mGluR5 can aggravate retinal lesions and vice versa. Similarly, Um et al. [27] also found that blocking mGluR5 with MTEP was able to relieve the behavioral disorder of rats in an AD model. In the rotenone-induced Parkinson's disease (PD) model, blockade of mGluR5 protected against neurotoxicity by mitigating oxidative stress-related DNA damage, ultimately improving the dyskinesia of rats in this PD model [28]. All of the above indicated a protective effect of inhibiting mGluR5 in various diseases, including DR.

Additionally, glutamate excitotoxicity has been suggested as a major factor triggering glaucoma and retinal cell damage [29], and retinal cell apoptosis is an important part of DR pathogenesis [30]. Notably, there was evidence that apoptosis in retinal vascular endothelial cells, pericytes, Muller, bipolar cell bodies, and retinal ganglion cells have been shown to result in impaired retinal microvascular structure, vascular leakage, and macular edema that eventually leads to retinal abnormality [31–33]. As reported by Park et al. [34], the retinal photoreceptor of STZ-induced rats appeared apoptotic at 4 weeks, and the number of apoptotic cells increased along with the extension of the disease as determined by the TUNEL assay. From our models, we also observed a large number of apoptotic cells in the inner nuclear and ganglion cell layers in rats from both the DM and DM + CHPG groups through the TUNEL assay, which was similar to the study of Barcelona et al. [35]. Additionally, the mGluR5 level and the apoptosis rate were increased in DM rats treated with CHPG, but the levels were decreased in rats treated with MTEP, implying that the activation of mGluR5 could induce retinal cell apoptosis and vice versa. A possible reason might be that the increase in glutamate concentration excessively activates mGluR5 to produce excitotoxicity, leading to the impairment of retinal function and apoptosis [36]. Consistently, Zhou et al. [37] found that mGluR5 expression level was significantly increased in rats with diabetic

neuropathic pain. In rat primary culture neuron model of Hodgkin's disease (HD), the activation of mGluR5 can give rise to the disorder of the calcium signaling pathway and cell apoptosis [38]. Moreover, the selective inhibition of mGluR5 by MPEP reduced the apoptosis of RGCs in a chronic hypertension rat model, as reported in a study by Zhao and his team [39]. As reported, DR has a negative effect on retinal function, leading to changes in the amplitude and peak time (a-wave and b-wave) in ERG tests [40]. Treatment with MTEP increased amplitude and shortened peak times, indicating that MTEP could improve retinal function in DR rats. To further clarify the mechanism of mGluR5 in DR, we have detected the oxidative stress-related index, and greatly reduced SOD activity and an obviously increased MDA level were identified in the serum and retinal tissues of DM rats. As is known from previous studies, hyperglycemia has been confirmed to cause the production of ROS and activate the oxidative stress response (which has been regarded as a common pathogenetic pathway for various diabetic complications) [35, 41]. To be specific, SOD activity eliminates free oxygen radicals [42], and MDA indirectly reflects the damage caused by free radical injury [43]. After blocking mGluR5 by MTEP, we found an increase in SOD activity and a decrease in MDA level, but the opposite results were exhibited after activation of mGluR5, suggesting that inhibition of mGluR5 could increase the antioxidant capacity of DR rats. Additionally, extracellular stimulation, such as hyperglycemia and oxidative stress, can phosphorylate JNK to generate p-JNK to activate the transcription factor AP-1 protein (c-Jun, c-Fos, and so on) and the downstream caspases, thereby triggering the apoptosis death receptor pathway and leading to cell apoptosis [44–46]. Our findings further revealed that activation of mGluR5 increases JNK pathway activity, but the inhibition of mGluR5 decreases JNK pathway activity. Moreover, Zhao et al. [47] reported that CHPG activates mGluR5, which activates the JNK signaling pathway in neurons. As reported by Fukuda and his group, knockout of the *JNK* gene obviously reduced the blood glucose level of STZ-induced hyperglycemic rats and decreased the apoptosis of islet cells induced by hyperglycemia [48]. More importantly, our findings also demonstrated that the body weight was significantly raised, and the blood glucose level was evidently reduced in DM rats and in DM rats treated with MTEP. All these results suggest that the inhibition of mGluR5 may suppress the downstream JNK pathway to reduce the blood glucose of diabetic rats, decrease diabetic retinal cell apoptosis, and increase antioxidant capacity, thus improving retinopathy damage.

In summary, mGluR5 was upregulated in DR rats, and the inhibition of mGluR5 can relieve DR via inhibiting the JNK signaling pathway, which provides a scientific basis for DR treatment.

Acknowledgements The authors appreciate the reviewers for their useful comments in this paper.

Compliance with ethical standards

Conflict of interest No potential conflicts of interest were disclosed.

Ethical approval The animal experimental design used in this study was approved by the Experimental Animal Ethics Committee of the First People's Hospital of Jingzhou; all experimental animal behaviors strictly followed the laboratory animal management and operation guide issued by the National Institutes of Health.

References

1. El-Asrar AM (2012) Role of inflammation in the pathogenesis of diabetic retinopathy. Middle East Afr J Ophthalmol 19:70–74
2. Yau JW, Rogers SL, Kawasaki R, Lamoureux EL, Kowalski JW et al (2012) Global prevalence and major risk factors of diabetic retinopathy. Diabetes Care 35:556–564
3. Huang H, He J, Johnson D, Wei Y, Liu Y et al (2015) Deletion of placental growth factor prevents diabetic retinopathy and is associated with Akt activation and HIF1α-VEGF pathway inhibition. Diabetes 64:200–212
4. Saxena R, Singh D, Saklani R, Gupta SK (2016) Clinical biomarkers and molecular basis for optimized treatment of diabetic retinopathy: current status and future prospects. Eye Brain 8:1–13
5. Wen D, Song W, Liu S, Tan X, Liu F (2015) Upregulated expression of N-methyl-D-aspartate receptor 1 and nitric oxide synthase during form-deprivation myopia in guinea pigs. Int J Clin Exp Pathol 8:3819–3826
6. Ji M, Miao Y, Dong LD, Chen J, Mo XF et al (2012) Group I mGluR-mediated inhibition of Kir channels contributes to retinal Muller cell gliosis in a rat chronic ocular hypertension model. J Neurosci 32:12744–12755
7. Alexander GM, Godwin DW (2006) Metabotropic glutamate receptors as a strategic target for the treatment of epilepsy. Epilepsy Res 71:1–22
8. Gerber U, Gee CE, Benquet P (2007) Metabotropic glutamate receptors: intracellular signaling pathways. Curr Opin Pharmacol 7:56–61

9. Gao F, Li F, Miao Y, Dong LD, Zhang SH et al (2015) Group I metabotropic glutamate receptor agonist DHPG modulates Kir4.1 protein and mRNA in cultured rat retinal Muller cells. Neurosci Lett 588:12–17
10. Yang L, Mao L, Chen H, Catavsan M, Kozinn J et al (2006) A signaling mechanism from Gαq-protein-coupled metabotropic glutamate receptors to gene expression: role of the c-Jun N-terminal kinase pathway. J Neurosci 26:971–980
11. Wagner EF, Nebreda AR (2009) Signal integration by JNK and p38 MAPK pathways in cancer development. Nat Rev Cancer 9:537–549
12. Chen F (2012) JNK-induced apoptosis, compensatory growth, and cancer stem cells. Cancer Res 72:379–386
13. Dhanasekaran DN, Reddy EP (2008) JNK signaling in apoptosis. Oncogene 27:6245–6251
14. Bayne K (1996) Revised guide for the care and use of laboratory animals available. American Physiological Society. Physiologist 39(199):111–208
15. Zheng Z, Chen H, Ke G, Fan Y, Zou H et al (2009) Protective effect of perindopril on diabetic retinopathy is associated with decreased vascular endothelial growth factor-to-pigment epithelium-derived factor ratio: involvement of a mitochondria-reactive oxygen species pathway. Diabetes 58:954–964
16. Yang H, Liu R, Cui Z, Chen ZQ, Yan S et al (2011) Functional characterization of 58-kilodalton inhibitor of protein kinase in protecting against diabetic retinopathy via the endoplasmic reticulum stress pathway. Mol Vis 17:78–84
17. Shi X, Liao S, Mi H, Guo C, Qi D et al (2012) Hesperidin prevents retinal and plasma abnormalities in streptozotocin-induced diabetic rats. Molecules 17:12868–12881
18. Chen W, Yao X, Zhou C, Zhang Z, Gui G et al (2017) Danhong huayu koufuye prevents diabetic retinopathy in streptozotocin-induced diabetic rats via antioxidation and anti-inflammation. Mediat Inflamm 2017:3059763
19. Rao VR, Prescott E, Shelke NB, Trivedi R, Thomas P et al (2010) Delivery of SAR 1118 to the retina via ophthalmic drops and its effectiveness in a rat streptozotocin (STZ) model of diabetic retinopathy (DR). Invest Ophthalmol Vis Sci 51:5198–5204
20. Liu N, Zhao N, Chen L, Cai N (2015) Survivin contributes to the progression of diabetic retinopathy through HIF-1α pathway. Int J Clin Exp Pathol 8:9161–9167
21. Mandarino LJ, Sundarraj N, Finlayson J, Hassell HR (1993) Regulation of fibronectin and laminin synthesis by retinal capillary endothelial cells and pericytes in vitro. Exp Eye Res 57:609–621
22. Choi JA, Chung YR, Byun HR, Park H, Koh JY et al (2017) The anti-ALS drug riluzole attenuates pericyte loss in the diabetic retinopathy of streptozotocin-treated mice. Toxicol Appl Pharmacol 315:80–89
23. Hammes HP (2005) Pericytes and the pathogenesis of diabetic retinopathy. Horm Metab Res 37(Suppl 1):39–43
24. Frank RN (2002) Potential new medical therapies for diabetic retinopathy: protein kinase C inhibitors. Am J Ophthalmol 133:693–698
25. Wisniewska-Kruk J, Klaassen I, Vogels IM, Magno AL, Lai CM et al (2014) Molecular analysis of blood-retinal barrier loss in the Akimba mouse, a model of advanced diabetic retinopathy. Exp Eye Res 122:123–131
26. Park SW, Yun JH, Kim JH, Kim KW, Cho CH et al (2014) Angiopoietin 2 induces pericyte apoptosis via α3β1 integrin signaling in diabetic retinopathy. Diabetes 63:3057–3068
27. Um JW, Kaufman AC, Kostylev M, Heiss JK, Stagi M et al (2013) Metabotropic glutamate receptor 5 is a coreceptor for Alzheimer aβ oligomer bound to cellular prion protein. Neuron 79:887–902
28. Xia N, Zhang Q, Wang ST, Gu L, Yang HM et al (2015) Blockade of metabotropic glutamate receptor 5 protects against DNA damage in a rotenone-induced Parkinson's disease model. Free Radic Biol Med 89:567–580
29. Schori H, Kipnis J, Yoles E, WoldeMussie E, Ruiz G et al (2001) Vaccination for protection of retinal ganglion cells against death from glutamate cytotoxicity and ocular hypertension: implications for glaucoma. Proc Natl Acad Sci USA 98:3398–3403
30. Chen K, Zhang Q, Wang J, Liu F, Mi M et al (2009) Taurine protects transformed rat retinal ganglion cells from hypoxia-induced apoptosis by preventing mitochondrial dysfunction. Brain Res 1279:131–138
31. Behl Y, Krothapalli P, Desta T, DiPiazza A, Roy S et al (2008) Diabetes-enhanced tumor necrosis factor-α production promotes apoptosis and the loss of retinal microvascular cells in type 1 and type 2 models of diabetic retinopathy. Am J Pathol 172:1411–1418
32. Geraldes P, Hiraoka-Yamamoto J, Matsumoto M, Clermont A, Leitges M et al (2009) Activation of PKC-delta and SHP-1 by hyperglycemia causes vascular cell apoptosis and diabetic retinopathy. Nat Med 15:1298–1306
33. Deng G, Moran EP, Cheng R, Matlock G, Zhou K et al (2017) Therapeutic effects of a novel agonist of peroxisome proliferator-activated receptor alpha for the treatment of diabetic retinopathy. Invest Ophthalmol Vis Sci 58:5030–5042
34. Park SH, Park JW, Park SJ, Kim KY, Chung JW et al (2003) Apoptotic death of photoreceptors in the streptozotocin-induced diabetic rat retina. Diabetologia 46:1260–1268
35. Barcelona PF, Sitaras N, Galan A, Esquiva G, Jmaeff S et al (2016) p75NTR and its ligand ProNGF activate paracrine mechanisms etiological to the vascular, inflammatory, and neurodegenerative pathologies of diabetic retinopathy. J Neurosci 36:8826–8841
36. Shen W, Fruttiger M, Zhu L, Chung SH, Barnett NL et al (2012) Conditional Mullercell ablation causes independent neuronal and vascular pathologies in a novel transgenic model. J Neurosci 32:15715–15727
37. Zhou CH, Zhang MX, Zhou SS, Li H, Gao J et al (2017) SIRT1 attenuates neuropathic pain by epigenetic regulation of mGluR1/5 expressions in type 2 diabetic rats. Pain 158:130–139
38. Zhang H, Li Q, Graham RK, Slow E, Hayden MR et al (2008) Full length mutant huntingtin is required for altered Ca2+ signaling and apoptosis of striatal neurons in the YAC mouse model of Huntington's disease. Neurobiol Dis 31:80–88
39. Zhao Y, Li Q, Li XY, Cui P, Gao F et al (2018) Involvement of mGluR I in EphB/ephrinB reverse signaling activation induced retinal ganglion cell apoptosis in a rat chronic hypertension model. Brain Res 1683:27–35

40. Lin BQ, Zhou JY, Ma Y, Deng YJ, Zheng CJ et al (2011) Preventive effect of danhong huayu koufuye on diabetic retinopathy in rats. Int J Ophthalmol 4:599–604
41. Dede AD, Tournis S, Dontas I, Trovas G (2014) Type 2 diabetes mellitus and fracture risk. Metabolism 63:1480–1490
42. Huang XP, Qiu YY, Wang B, Ding H, Tang YH et al (2014) Effects of Astragaloside IV combined with the active components of Panax notoginseng on oxidative stress injury and nuclear factor-erythroid 2-related factor 2/heme oxygenase-1 signaling pathway after cerebral ischemia-reperfusion in mice. Pharmacogn Mag 10:402–409
43. El Mesallamy HO, Metwally NS, Soliman MS, Ahmed KA, Abdel Moaty MM (2011) The chemopreventive effect of Ginkgo biloba and Silybum marianum extracts on hepatocarcinogenesis in rats. Cancer Cell Int 11:38
44. Tezel G, Chauhan BC, LeBlanc RP, Wax MB (2003) Immunohistochemical assessment of the glial mitogen-activated protein kinase activation in glaucoma. Invest Ophthalmol Vis Sci 44:3025–3033
45. Yang W, Tiffany-Castiglioni E, Koh HC, Son IH (2009) Paraquat activates the IRE1/ASK1/JNK cascade associated with apoptosis in human neuroblastoma SH-SY5Y cells. Toxicol Lett 191:203–210
46. Li X, Weng H, Xu C, Reece EA, Yang P (2012) Oxidative stress-induced JNK1/2 activation triggers proapoptotic signaling and apoptosis that leads to diabetic embryopathy. Diabetes 61:2084–2092
47. Zhao L, Jiao Q, Chen X, Yang P, Zhao B et al (2012) mGluR5 is involved in proliferation of rat neural progenitor cells exposed to hypoxia with activation of mitogen-activated protein kinase signaling pathway. J Neurosci Res 90:447–460
48. Fukuda K, Tesch GH, Nikolic-Paterson DJ (2008) c-Jun amino terminal kinase 1 deficient mice are protected from streptozotocin-induced islet injury. Biochem Biophys Res Commun 366:710–716